Appendix 1

Methods

The convolutional neural networks (CNNs) used in this study included: (I) shallow CNN (SCNN): the network structure contained three convolutional layers, namely 32×3×3, 64×3×3, and 128×3×3; each convolutional layer contained a pooling layer 2×2, the full connection layer 512×1 and the activation layer 1×1. (II) LeNet: the network structure of LeNet5 was used, including two convolutional layers, namely 16×5×5, and 32×5×5, and each convolutional layer contained a pooling layer 2×2, connecting two fully connected layers 512×1, and 256×1 and the last activation layer 1×1. (III) VGG16, ResNet50 and DenseNet121: these three models comprise a fully connected layer of 512 nodes, with the last single node of the network as the activation layer for pattern classification. The loss function for the model training was binary_crossentropy. The Relu function was used as the activation function of all convolutional layers. The sigmoid function was the final activation function of deep learning (DL) network, which was used for the binary classification of moyamoya angiopathy (MMA) *vs.* controls. The Adam algorithm was used to optimize the model. The learning rate was $10e^{-6}$, the Beta 1 value was 0.9, and the Beta 2 value was 0.999. The batch size of the model training was 32, and the training epochs were 20 (32-34). Generally, training epochs are set from tens to hundreds when training samples are large, such as the traditional data set of 60,000 samples, which makes the model more accurate. However, our training set was only 14,360 after the data was enhanced. High epochs are prone to overfitting effect caused by overtraining. Therefore, 20 epochs were set in this work.

References

32. Cao Z, Huang J, He X, Zong Z. BND-VGG-19: A deep learning algorithm for COVID-19 identification utilizing X-ray images. Knowl Based Syst 2022;258:110040.
33. Rai HM, Chatterjee K. 2D MRI image analysis and brain tumor detection using deep learning CNN model LeU-Net. Multimed Tools Appl 2021;80:36111-41.
34. Osman AFI, Tamam NM. Deep learning-based convolutional neural network for intramodality brain MRI synthesis. J Appl Clin Med Phys 2022;23:e13530.

https://dx.doi.org/10.21037/qims-24-1269

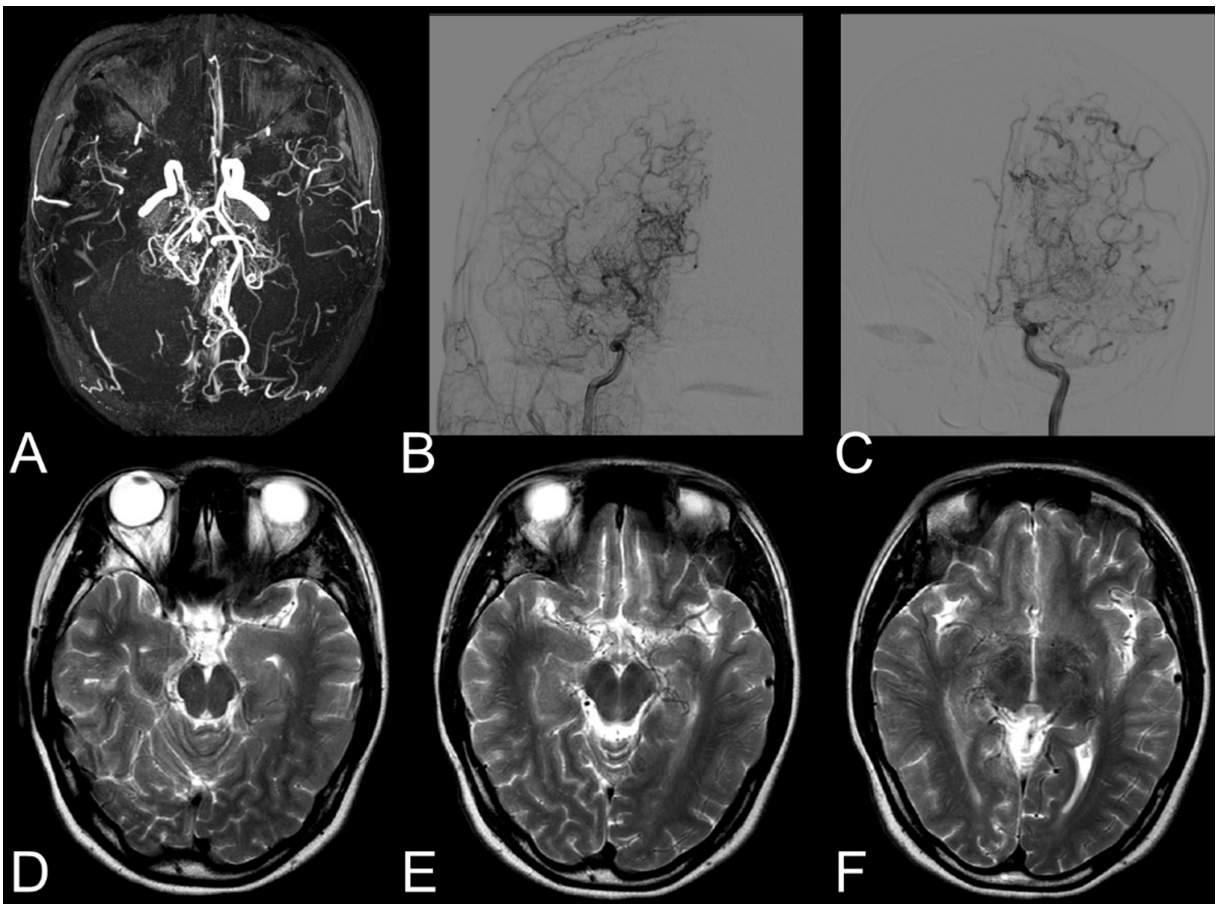

Figure S1 Images of a patient with moyamoya angiopathy. (A-C) magnetic resonance angiography and digital subtraction angiography images showing the occlusion of bilateral internal carotid artery, middle cerebral artery, and anterior cerebral artery with collateral information around. (D-F) three continuous slices of T2-weighted imaging at the central level of the basal cistern. Flow voids were found around the basal cistern.

https://dx.doi.org/10.21037/qims-24-1269

Table S1 MR scanner, acquisition coil and parameters of T2-weighted images and 3D TOF MRA in 7 sites

Site	MR scanner	Coil	T2WI				3D TOF MRA	
			Acquisition sequence	TR (ms)/TE (ms) /FA (°)	Thickness (mm)/slice gap	Voxel size (mm^2)	TR (ms)/TE (ms)/FA (°)	Voxel size (mm^3)
Site 1	Philips Ingenia CX 3.0T	32	TFE	2,200/30/90	6/7	0.5*0.8	22/3.5/18	0.6*0.93*1
	Philips Achieva TX 3.0T	16	TSE	2,332/80/90	6/7	0.3*0.3	25/3.5/30	0.4*0.4*1.4
	Philips Achieva 1.5T	16	TSE	2,020/100/90	6/7	0.5*0.5	23/6.9/20	0.5*0.5*1.4
	UIH UMR770 3.0T	24	FSE	4,566/107/130	6/7.2	0.8*0.8	18.8/3.4/17	0.3*0.3*0.6
	GE Signa 1.5T	8	FSE	4,750/115.5/160	6/7	0.5*0.5	23/6.8/18	0.5*0.5*1.4
Site 2	Siemens Verio 3.0T	32	TSE	6,000/95/150	5/6.5	0.6*0.6	21/3.45/18	0.3*0.3*0.5
Site 3	Siemens Verio 3.0T	8	TSE	3,020/90/150	5/6.5	0.4*0.4	19/3.5/15	0.6*0.6*0.8
	Siemens Avanto 1.5T	8	TSE	2,850/99/150	6/7.8	1*0.7	26/7/25	0.6*0.6*0.7
Site 4	Siemens Verio 3.0T	8	TSE	3,500/106/150	6/7.8	0.6*0.6	20/3.6/18	0.5*0.5*1
	GE Signa 1.5T	8	FSE	4,000/103.4/90	6/8	0.5*0.5	27/3.5/16	0.4*0.4*1.6
	GE MR750 3.0T	32	FSE	4,126/126/142	6/8	0.5*0.5	21/2.4/20	0.5*0.5*1.4
Site 5	GE MR750 3.0T	32	FSE	5,048/120/142	5/6.5	0.4*0.4	25/3.4/20	0.4*0.4*1.4
	Siemens TrioTim 3.0T	16	TSE	4,000/98/120	5/6.5	0.5*0.5	21/3.6/18	0.3*0.3*0.5
	Siemens Magnetom_ essenza 1.5T	8	TSE	3,300/109/150	5/6.5	0.6*0.6	27/6/22	0.3*0.3*0.8
	GE Genesis_signa 1.5T	8	FSE	3,500/102/90	5/6.5	0.5*0.5	34/3.9/20	0.4*0.4*1.2
Site 6	UIH UMR770 3.0T	24	FSE	3,970/98.4/145	5.5/6.6	0.6*0.6	16.8/3.6/20	0.4*0.4*0.5
	Philips Achieva 1.5T	8	TSE	1,788/110/90	7/7.5	0.7*0.7	25/6.9/20	0.3*0.3*0.6
Site 7	Philips Ingenia 3.0T	16	TSE	4,000/110/90	5/6	0.8*0.8	22/3.5/18	0.7*1*1.5
	Siemens Avanto 1.5T	16	TSE	6,270/139/150	5.5/6.1	0.9*0.9	25/7/25	0.4*0.4*0.6

Site 1, Nanjing Drum Tower Hospital, Affiliated Hospital of Medical School, Nanjing University; site 2, The Affiliated Sir Run Run Hospital of Nanjing Medical University; site 3, Xuyi People's Hospital; site 4, the Affiliated Brain Hospital of Nanjing Medical University; site 5, Jinling Hospital, Affiliated Hospital of Medical School, Nanjing University; site 6, Lu'an Hospital of Anhui Medical University; site 7, Children's Hospital of Nanjing Medical University. MR, magnetic resonance; T2WI, T2-weighted imaging; 3D TOF MRA, three-dimensional time-of-flight magnetic resonance angiography; TR, repetition time; TE, echo time; FA, flip angle; TFE, turbo field echo; TSE, turbo spin echo; FSE, fast spin echo.

https://dx.doi.org/10.21037/qims-24-1269

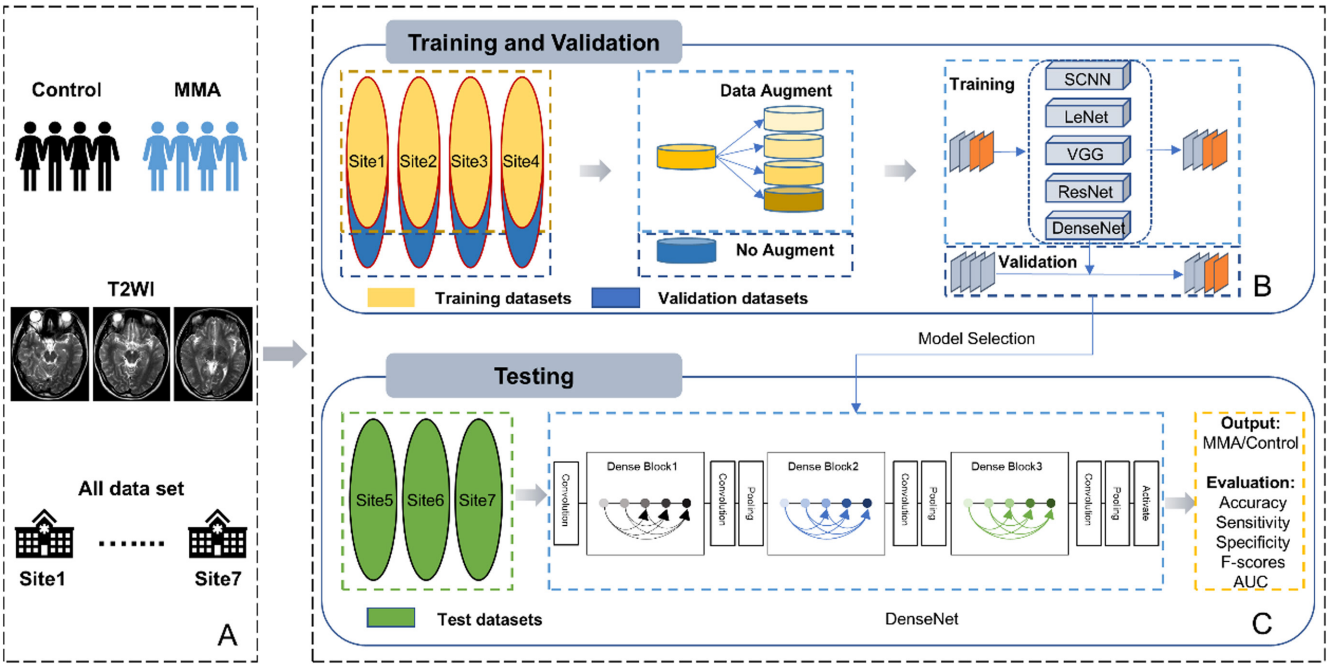

Figure S2 Training and testing workflow. (A) Model input. (B) Training and internal validation stage in sites 1–4. (C) Testing stage: external validation in sites 5–7. Site 1, Nanjing Drum Tower Hospital, Affiliated Hospital of Medical School, Nanjing University; site 2, The Affiliated Sir Run Run Hospital of Nanjing Medical University; site 3, Xuyi People's Hospital; site 4, the Affiliated Brain Hospital of Nanjing Medical University; site 5, Jinling Hospital, Affiliated Hospital of Medical School, Nanjing University; site 6, Lu'an Hospital of Anhui Medical University; site 7, Children's Hospital of Nanjing Medical University. MMA, moyamoya angiopathy; T2WI, T2-weighted imaging; AUC, area under the curve; SCNN, shallow convolutional neural network; LeNet, LeNet-5 Convolutional Neural Network; VGG, Visual Geometry Group Network; ResNet, Residual Neural Network; DenseNet, Dense Convolutional Network.

https://dx.doi.org/10.21037/qims-24-1269

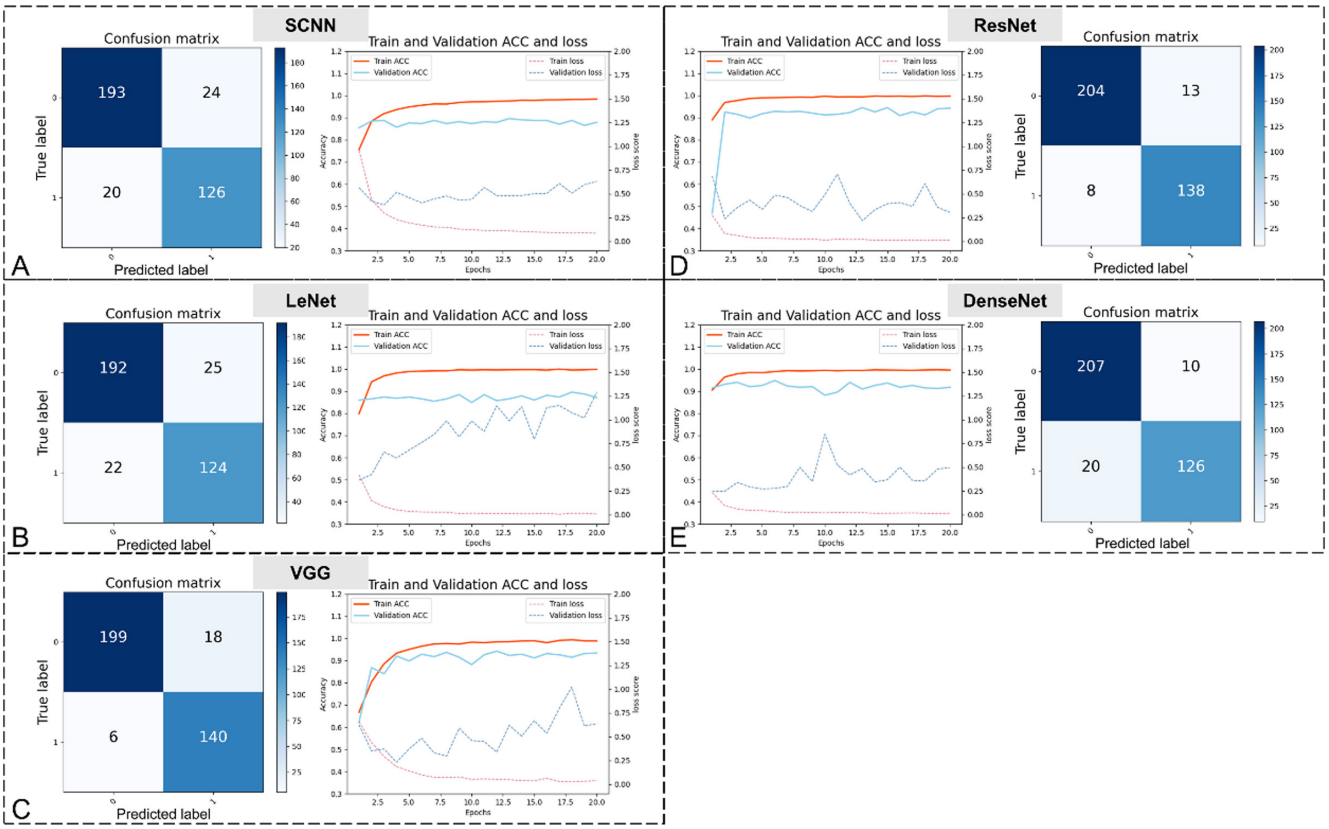

Figure S3 Confusion matrix, accuracy and loss curves of internal validation data set for SCNN (A), LeNet (B), VGG (C), ResNet (D) and DenseNet (E). SCNN, shallow convolutional neural network; LeNet, LeNet-5 Convolutional Neural Network; VGG, Visual Geometry Group Network; ResNet, Residual Neural Network; DenseNet, Dense Convolutional Network; ACC, accuracy.

https://dx.doi.org/10.21037/qims-24-1269

Table S2 Results of SCNN, LeNet, VGG, ResNet and DenseNet in the external validation data set

Model	Test data	Sensitivity	Specificity	F1 score	Accuracy	AUC-ROC
SCNN	Site 5	0.761 (0.703, 0.817)	0.549 (0.496, 0.601)	0.627	0.63 (0.591, 0.669)	0.687
	Site 6	0.434 (0.232, 0.637)	0.763 (0.628, 0.898)	0.647	0.639 (0.518, 0.759)	0.621
	Site 7	0.527 (0.375, 0.670)	0.705 (0.590, 0.819)	0.63	0.628 (0.536, 0.721)	0.721
	Total	0.697 (0.644, 0.751)	0.588 (0.543, 0.634)	0.626	0.631 (0.595, 0.665)	0.682
LeNet	Site 5	0.797 (0.743, 0.851)	0.347 (0.297, 0.397)	0.534	0.521 (0.479, 0.561)	0.611
	Site 6	0.478 (0.274, 0.682)	0.842 (0.726, 0.958)	0.716	0.705 (0.591, 0.819)	0.734
	Site 7	0.545 (0.398, 0.692)	0.836 (0.743, 0.929)	0.721	0.714 (0.627, 0.801)	0.711
	Total	0.732 (0.681, 0.783)	0.456 (0.410, 0.503)	0.564	0.563 (0.527, 0.599)	0.624
VGG	Site 5	0.834 (0.784, 0.883)	0.816 (0.775, 0.856)	0.821	0.823 (0.791, 0.854)	0.882
	Site 6	0.608 (0.410, 0.808)	0.970 (0.922, 0.998)	0.845	0.836 (0.743, 0.928)	0.857
	Site 7	0.886 (0.792, 0.980)	0.901 (0.826, 0.976)	0.894	0.893 (0.836, 0.953)	0.942
	Total	0.823 (0.779, 0.868)	0.841 (0.807, 0.875)	0.833	0.834 (0.807, 0.861)	0.886
ResNet	Site 5	0.829 (0.779, 0.878)	0.891 (0.858, 0.923)	0.867	0.867 (0.839, 0.895)	0.921
	Site 6	0.448 (0.232, 0.637)	0.973 (0.920, 0.990)	0.771	0.795 (0.664, 0.876)	0.818
	Site 7	0.727 (0.595, 0.858)	0.918 (0.849, 0.986)	0.84	0.838 (0.767, 0.908)	0.922
	Total	0.782 (0.736, 0.829)	0.901 (0.873, 0.929)	0.855	0.855 (0.829, 0.880)	0.903
DenseNet	Site 5	0.875 (0.831, 0.915)	0.844 (0.806, 0.883)	0.855	0.856 (0.827, 0.885)	0.936
	Site 6	0.57 (0.362, 0.768)	0.970 (0.927, 0.991)	0.832	0.819 (0.723, 0.916)	0.869
	Site 7	0.863 (0.762, 0.965)	0.918 (0.849, 0.986)	0.895	0.894 (0.836, 0.953)	0.935
	Total	0.848 (0.806, 0.890)	0.865 (0.834, 0.897)	0.858	0.859 (0.833, 0.884)	0.925

The data were expressed as mean or mean (95% confidence interval). Site 5, Jinling Hospital, Affiliated Hospital of Medical School, Nanjing University; site 6, Lu'an Hospital of Anhui Medical University; site 7, Children's Hospital of Nanjing Medical University. AUC, area under the curve; ROC, receiver operating characteristic; SCNN: shallow convolutional neural network; LeNet, LeNet-5 Convolutional Neural Network; VGG, Visual Geometry Group Network; ResNet, Residual Neural Network; DenseNet, Dense Convolutional Network.

https://dx.doi.org/10.21037/qims-24-1269

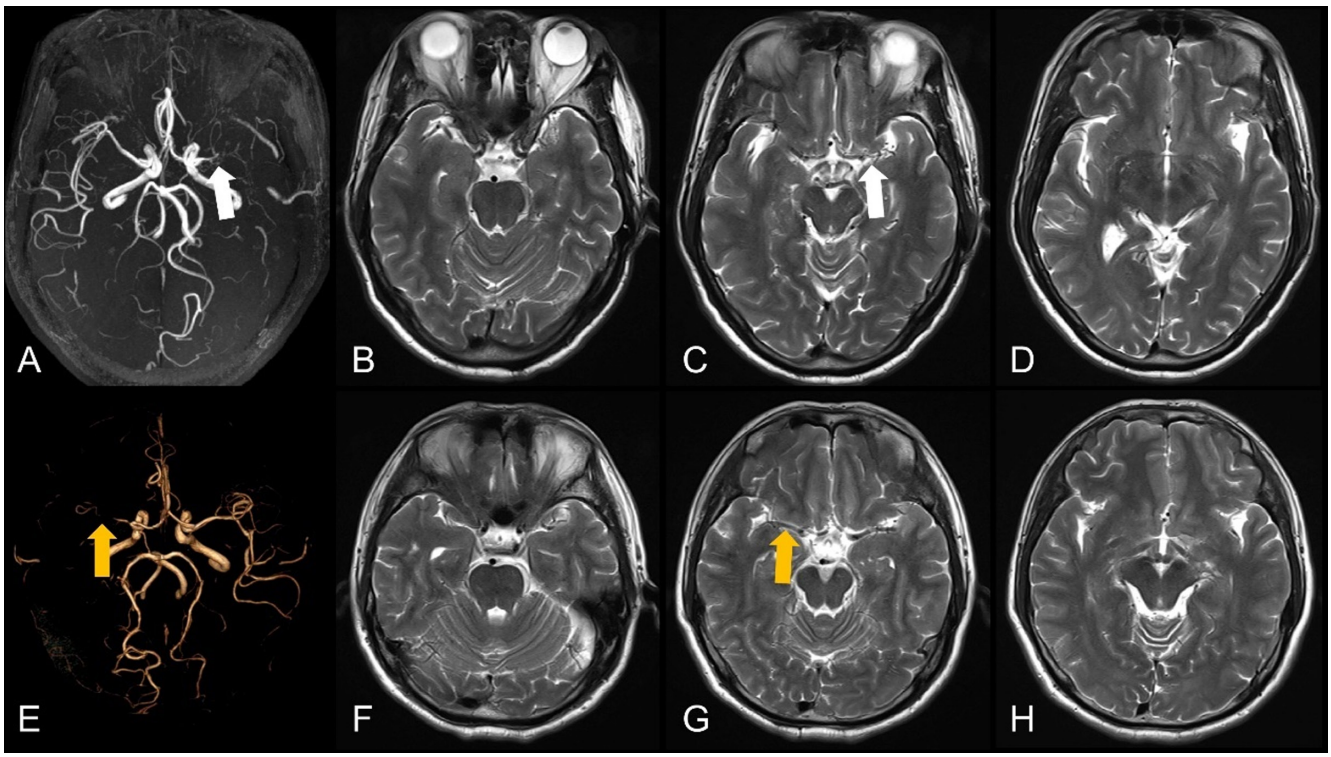

Figure S4 Missed and misdiagnosed cases of Dense Convolutional Network model in site 5 (Site 5, Jinling Hospital, Affiliated Hospital of Medical School, Nanjing University). (A-D) A 62-year-old male with left MMA, who was missed. MRA (A: maximum intensity projection) revealed the occlusion of the left middle cerebral artery (white arrow) with surrounded collaterals. (B-D) T2WI at the central level of the basal cistern. The M1 segment of the left middle cerebral artery disappeared with surrounded flow voids (white arrow in C). (E-H) A 54-year-old male patient, who was misdiagnosed as MMA. MRA (E: volume rendering) shows a narrowing of the M1 segment of the right middle cerebral artery (yellow arrow) with no evident collateral circulation. (F-H) T2WI at the central level of the basal cistern. The M1 segment of the right middle cerebral artery is shown in G (yellow arrow). MMA, moyamoya angiopathy; MRA, magnetic resonance angiography; T2WI, T2-weighted imaging.

https://dx.doi.org/10.21037/qims-24-1269

Table S3 Diagnostic performance of radiologists and DenseNet based on data from site 5

Category	Sensitivity	Specificity	F1 score	Accuracy	AUC
Radiologist 1	0.949 (0.920, 0.978)	0.075 (0.047, 0.102)	0.512	0.411 (0.370, 0.451)	0.512
1.5 T	0.954 (0.914, 0.993)	0.083 (0.038, 0.128)	0.599	0.455 (0.393, 0.516)	0.518
3.0 T	0.945 (0.902, 0.988)	0.069 (0.034, 0.104)	0.514	0.375 (0.321, 0.429)	0.507
Radiologist 2	0.650 (0.586, 0.713)	0.994 (0.986, 1.0)	0.783	0.862 (0.834, 0.890)	0.822
1.5 T	0.611 (0.519, 0.703)	0.986 (0.967, 1.0)	0.799	0.826 (0.779, 0.873)	0.799
3.0 T	0.688 (0.601, 0.775)	1.0 (1.0, 1.0)	0.815	0.891 (0.856, 0.926)	0.844
DenseNet	0.876 (0.832, 0.919)	0.845 (0.807, 0.883)	0.824	0.857 (0.828, 0.886)	0.860
1.5 T	0.907 (0.853, 0.962)	0.917 (0.872, 0.962)	0.899	0.913 (0.878, 0.948)	0.912
3.0 T	0.844 (0.776, 0.912)	0.793 (0.737, 0.849)	0.757	0.811 (0.767, 0.854)	0.819

The data were expressed as mean or mean (95% confidence interval). The radiologists' diagnoses were based on three T2-weighted image slices from the site 5 dataset. They were asked to assess the presence of moyamoya angiopathy (moyamoya angiopathy/control). Site 5, Jinling Hospital, Affiliated Hospital of Medical School, Nanjing University. AUC, area under the curve; DenseNet, Dense Convolutional Network.

Table S4 The accuracy comparison between radiologists and DenseNet across different MRA score ranges

Category	MRA score		
	≤5	6–10	≥11
Radiologist 1	0.956 (0.907, 1.0)	0.952 (0.912, 0.993)	0.932 (0.857, 1.0)
Radiologist 2	0.618 (0.502, 0.733)	0.638 (0.546, 0.730)	0.727 (0.596, 0.859)
DenseNet	0.750 (0.647, 0.853)	0.924 (0.873, 0.975)	0.955 (0.893, 1.0)
P1	0.001	0.390	0.645
P2	0.097	<0.001	0.004

The data were expressed as mean (95% confidence interval). P1 and P2 represent the accuracy comparisons of radiologists 1 and 2 versus DenseNet in moyamoya angiopathy patients across MRA score ranges (≤5, 6–10, ≥11) using a two-proportion z-test. DenseNet, Dense Convolutional Network; MRA, magnetic resonance angiography.

https://dx.doi.org/10.21037/qims-24-1269